

RESEARCH

Open Access



Computed tomographic features of pulmonary pure ground-glass nodule: a comparison between neoplastic and non-neoplastic nodules

Mona Ahmed Fouad Hafez^{1*} , Arwa Mohammed Abdulbaset Emam Elgaml¹, Mostafa Ahmed Khairy¹, Yasmine Hamdy El Hinnawy² and Mohammed Raafat Abd-Elmageed¹

Abstract

Background: Ground-glass nodules (GGNs) are detected more frequently nowadays with the increase in MDCT resolution and applications. On CT GGN is a well circumscribed nodule with mild increase attenuation and not obscuring bronchial and vascular markings. This study aimed to discriminate neoplastic from non-neoplastic pure ground-glass nodules (pGGNs) by performing comparative quantitative and qualitative assessment of main features in computed tomography (CT) chest imaging. This prospective study involved 72 patients, who were referred to perform multidetector computed tomography of the chest in the radiology department. Cases with ground-glass pulmonary nodules were included in the study, and each nodule was assessed and followed for 2 years by a radiomics software for density and histogram analysis and then classified to neoplastic and non-neoplastic nodules. Neoplastic and non-neoplastic nodules morphology and radiomics were compared, and statistical analysis was done.

Results: After histopathology, positron emission tomography and computed tomography, or close follow-up, pGGNs were classified to neoplastic and non-neoplastic nodules. There was statistically significant difference regarding the mean size, where in cases of neoplastic nodules it was 6.66 mm and the mean size of benign nodules was 11.25 mm. Moreover, irregularity index and histogram peak frequency had a significant correlation with a P value of 0.007 and 0.022, respectively. The cutoff level for peak frequency percentage was 20.5% with 56.3% sensitivity and 79.2% specificity.

Conclusions: Radiomics had a growing role in pulmonary nodule assessment. Radiomics along with morphologic features assessment improved the detection efficiency of neoplastic versus non-neoplastic ground-glass nodules with histogram peak frequency, nodule size, and irregularity index as the main differentiating factors in this study.

Keywords: Ground glass, Pulmonary nodules, CT chest, Histogram

Background

Lung nodules are classified into three types: solid, part-solid, and nonsolid or ground-glass nodules (GGNs) [1]. The GGNs are classified into pure ground-glass nodules (pGGNs) and part-solid nodule [2].

The differential diagnosis of lung nodules carries wide varieties of non-neoplastic and neoplastic causes. Lung cancer is one of the most common malignant tumors in

*Correspondence: mona.fouad@kasralainy.edu.eg

¹ Diagnostic Radiology and Intervention Department, Kasr Al-Ainy Faculty of Medicine - Cairo University, Al-Manial, Cairo 11559, Egypt
Full list of author information is available at the end of the article

the world and the leading cause of cancer-related death worldwide [3]. It is difficult to differentiate the diagnosis of pulmonary nodules even at follow-up. Preinvasive adenocarcinoma (PIA), including atypical adenomatous hyperplasia (AAH), adenocarcinoma in situ (AIS), and invasive adenocarcinoma (IAC), including minimally IAC (MIA), can often appear as GGNs and may not enlarge for several months or more. However, inflammatory GGN lesions often regress and resolve spontaneously or after treatment with antibiotics [4].

The advent of CT screening for lung cancer has increased the incidence of GGNs. The persistence of nodular GGNs over time is strongly suggestive of an early-stage malignancy, especially if the lesion increases in size or includes a solid component that increases in its extent. The more extensive the solid portions of the lesion, the higher the probability of malignancy and the poorer the prognosis. Although GGNs have a probability of malignancy, a few lesions were benign. Most of non-neoplastic GGNs are transient as inflammation, and hemorrhage and a small number of persistent lesions are finally confirmed as focal interstitial fibrosis. These GGNs are often misdiagnosed as lung cancers and treated by unnecessary surgical resection. Therefore, carefully discriminating benign GGNs from malignant ones remains a challenge [5, 6].

An awareness of the clinical setting, in addition to familiarity with the thin-section CT features of nodular GGNs at initial and follow-up imaging over several months, can help to identify malignancy and achieve an accurate diagnosis. A meticulous evaluation of those CT features, and their correlation with specific histopathologic characteristics, may also enable a more accurate prognosis in cases of neoplastic disease [6].

Radiomics refers to the process of imaging feature extraction and quantitative analysis of tumor heterogeneity by analyzing the distribution and relationship of pixel or voxel gray levels in the image. For various tumors, there are quantifiable texture differences between benign and malignant lesions (generally with greater heterogeneity in malignant lesions), possibly allowing pathologic differentiation in certain clinical scenarios [7].

This study aimed to evaluate and compare qualitatively and quantitatively neoplastic from non-neoplastic pure ground-glass nodules (pGGNs).

Methods

Study population

This prospective study was conducted according to the guidelines of the Ethics Committee and was approved by its Institutional Review Board. During the period from March 2018 to June 2021, after exclusion of solid and part-solid pulmonary nodules, and cases off-track

their follow-up, and inclusion of cases with pGGNs, 72 patients fulfilled the inclusion criteria, where 46 were females and 26 males and age ranged from 27 to 94 years old. Informed written consents were obtained from all cases prior to enrollment. All cases are then subjected to thorough clinical examination with history taking, general and chest examination, and non-enhanced computed tomography (NECT), and all cases were followed with NECT for up to 2 years.

The final diagnosis of nodules was concluded according to histopathological assessment in 15 cases; when malignancy was suspected by primary features, PET-CT assessment in 28 cases in equivocal cases more than 8 mm in diameter, and follow-up in 29 cases; when benign features were suspected in initial CT.

CT chest study

All patients performed CT scans at a 16-multidetector CT (MDCT) scanner.

Patients were scanned during full end of inspiration in supine position. No intravenous contrast injection was introduced.

Contiguous axial slices of CT scans were performed to all patients using Siemens 16 channel MDCT. No preparation needed. Non contrast helical-volumetric axial cuts were performed in full inspiration in supine position with 1.5 mm slice thickness, 1.5 mm pitch, 0 gantry tilt, FOV depending on patient size around 320 mm from root of neck to the level of renal arteries, KV 120, mAs 25, Rotation time 0.5 s, total exposure time 8–10 s, HRCT window width (WW) was 1000 HU and window level (WL) was -700 and mediastinal WW was 300 HU, WL was 30 HU.

Data analysis

- The morphological characteristics were analyzed and by two conjoint radiologists of 16 and 10 years of chest radiology experience, blinded from clinical data.
- Each pGGN was assessed regarding nodule location (central, peripheral, subpleural, and subfissural); number (solitary and multiple); shape (regular, rounded, oval or irregular, speculated, stellate, and angulated); and margin (well-defined or ill-defined/blur margin).

Nodule segmentation and histogram analysis

- Each selected pGGN was evaluated using a commercially available workstation (Advantage Workstation GE Healthcare) by its lung analysis software

(Lung VCAR; GE Healthcare). Lung nodules were semiautomated segmented by the software based on ground-glass attenuation value.

- Semiautomatic region of interest (ROI) was applied covering the largest possible area of each nodule, and the large vessels and pulmonary arteries were excluded from the ROIs. This process was repeated for each contiguous transverse level until the entire tumor had been covered. Voxel-based CT numbers were then collected from the lesion segmentation.
- The qualitative and quantitative measures for histogram, texture, and geometric features of ROI were extracted.
 - The maximum and minimum sizes of the GGNs with the irregularity index are measured, the size of the nodule is measured manually as the short-axis (minimum) and long-axis (maximum) diameter, and the irregularity index is the maximum/minimum diameter.
 - Visual assessment of the GGN histogram (α , β): α represented histogram with sharp peak at low CT value and β represented histogram with no sharp peak at low CT value.
 - Mean, minimum, and maximum density and histogram of the GGN: the computer automatically calculated the density from the mean attenuation of the total voxels and volume by multiplying the number of voxels by the unit volume of a voxel.
 - Peak CT number (PEAK), peak frequency percentage, and number of peaks of the histogram were measured. Peak means the most frequent CT number of the most pixels within the whole nodule corresponding to the highest bar in CT number histogram of nodule.
 - Skewness represented the degree of the asymmetric tail extending toward either the high or low CT value. The GGNs divided the nodules into three categories based on the visual assessment of CT histograms (negative skewed distribution to the left, symmetric skewness, and positive skewed distribution to the right).
 - Kurtosis (peakedness/flatness of pixel histogram): GGNs were divided into kurtosis less than 0, equals 0, and more than 0.

Follow-up and final diagnosis

- Two years of follow-up with further assessment of the selected nodule was performed for all cases by HRCT chest.

- Nodules were classified into neoplastic and non-neoplastic nodules according to histopathology as follows: if suspected neoplastic and for progressive nodules on follow-up, PET-CT, and close follow-up for suspected benign nodules; nodules that showed regressive course diagnosed as benign and nodules with progressive changes diagnosed as neoplastic.

Statistical analysis

Data were coded and entered using the statistical package SPSS (Statistical Package for the Social Sciences) version 28 (IBM Corp., Armonk, NY, USA). Data were summarized using mean, standard deviation, median, minimum and maximum in quantitative data and using frequency (count) and relative frequency (percentage) for categorical data, when their distribution found parametric.

For comparison of paired measurements within each patient the nonparametric Wilcoxon signed rank test was used in numerical data and the nonparametric McNemar test and Marginal Homogeneity Test were used in nominal data. For comparing categorical data, Chi square (χ^2) test was performed. Exact test was used instead when the expected frequency is less than 5. P value less than 0.05 was considered as statistically significant.

Results

Patient profiles

This study involved 72 patients: 46 females (64%) and 26 males (36%). Age ranged from 27 to 94 years, with mean age 55.57 (S.D. \pm 15.64).

A total of 24 GGNs (33.3%) were diagnosed as benign nodules and 48 GGNs (66.7%) as neoplastic nodules. Of the neoplastic nodules, 29.2% were primary lung tumor, while 70.8% of neoplastic nodules were metastatic mainly from breast and pancreatic cancers.

The mean age for benign nodules was 51.42 years and 57.65 years for neoplastic nodules. There was no significant difference in the mean age between patients with neoplastic and non-neoplastic nodules.

Each segmented GGN was assessed, and correlation between neoplastic and non-neoplastic nodules was done.

According to pGGNs location and morphological characters

Most of the pGGNs were peripheral rather than central with subpleural/subfissural, and upper lobe location was significantly related to benign nodules.

Regular-shaped and well-defined nodules had a significant positive relationship of increasing their susceptibility to be neoplastic (P -value 0.019 and <0.001 , respectively) (Table 1).

Table 1 Distribution and relation between the neoplastic and non-neoplastic segmented pGGNs in CT scan regarding their location, shape, and margin

	Total GGNs		Diagnosis				P-value
			Benign N = 24		Malignant N = 48		
	Count	%	Count	%	Count	%	
Central distribution	6	8.3%	4	16.7%	2	4.2%	0.091
Peripheral distribution	64	88.9%	20	83.3%	44	91.7%	0.427
Subpleural/subfissural	38	52.8%	18	75.0%	20	41.7%	0.008*
Upper lobe	32	44.4%	16	66.7%	16	33.3%	0.007*
Middle lobe/lingula	15	20.8%	2	8.3%	13	27.1%	0.065
Lower lobe	24	33.3%	6	25.0%	18	37.5%	0.289
Right	56	77.8%	21	87.5%	35	72.9%	0.161
Left	18	25.0%	3	12.5%	15	31.3%	0.083
Solitary	2	4.2%	0	0.0%	2	4.2%	0.549
Multiple	70	95.8%	24	100.0%	46	95.8%	0.549
Regular rounded	29	40.3%	2	8.3%	27	56.3%	<0.001**
Irregular speculated-angulated	44	61.1%	22	91.7%	22	45.8%	<0.001**
Well-defined (margin)	38	52.8%	8	33.3%	30	62.5%	0.019*
Ill-Defined (margin)	34	47.2%	16	66.7%	18	37.5%	0.019*

P-value > 0.05 NS; *P-value < 0.05 S; **P-value < 0.001 HS

Size and irregularity index of GGNs

There was statistically significant relation between the final diagnosis of lung nodule with size and irregularity index (P-value of 0.007). Mean long-axis diameter in cases of neoplastic nodules was 6.66 mm in maximum nodule diameter, but the mean size of benign nodules was 11.25 mm in maximum nodule diameter (P value of 0.002) (Table 2).

The cutoff levels regarding the size and irregularity index of nodule were calculated to detect its type (CI = 95%) using receiver operating characteristic (ROC) curve. Nodule size cutoff was 8.8 mm with sensitivity and

specificity of 74.5% and 62.5%, respectively. Irregularity index cutoff level was 1.9032 with sensitivity and specificity of 78.7% and 54.2%, respectively (Table 3) (Fig. 1), with distribution of neoplastic and non-neoplastic nodules displayed in Fig. 2.

GGNs density and histogram analysis

In histogram analysis, with the mean, minimum, and maximum density of neoplastic and non-neoplastic nodules with mean density displayed in Fig. 2, there was no significant relation between mean density and the type of nodule. However, that peak frequency had a significant

Table 2 Relation between nodule size and irregularity index in CT scan with the final diagnosis

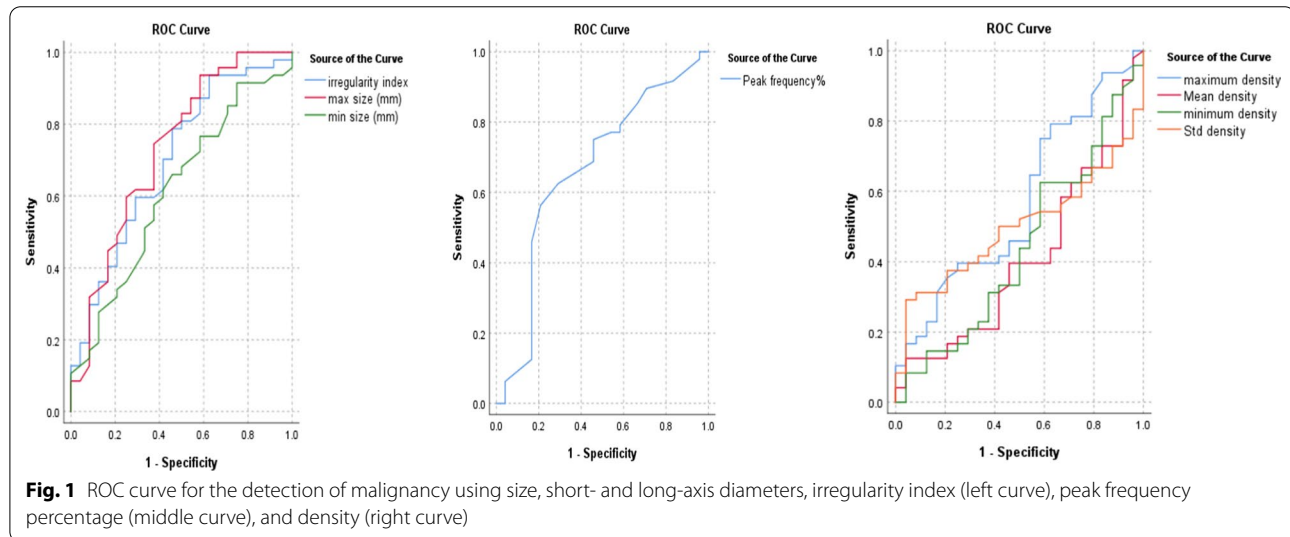
	Diagnosis										P-value
	Benign					Malignant					
	Mean	SD	Median	Minimum	Maximum	Mean	SD	Median	Minimum	Maximum	
Long-axis diameter (mm)	11.25	6.15	10.05	3.30	22.90	6.66	3.53	5.80	2.10	16.60	0.002*
Short-axis diameter (mm)	4.98	1.97	4.70	2.00	8.30	4.26	2.04	3.60	1.30	10.10	0.118
Irregularity index	2.30	1.10	1.94	1.10	5.09	1.92	2.27	1.49	0.93	16.62	0.007*
Mean density	−501.08	113.50	−473.95	−673.40	−261.30	−470.68	120.10	−446.50	−824.20	−261.30	0.201
Maximum density	−263.50	123.46	−278.00	−532.00	−6.00	−307.71	149.13	−266.00	−689.00	−65.00	0.351
Minimum density	−764.96	104.84	−782.50	−1,015.00	−584.00	−743.35	109.44	−752.00	−989.00	−470.00	0.403
Std density	99.60	23.86	100.35	51.10	154.30	103.95	40.86	98.15	43.70	190.00	0.952
Peak frequency%	18.25	7.81	17.00	9.00	41.00	21.13	6.26	21.00	10.00	35.00	0.022*

P-value > 0.05 NS; *P-value < 0.05 S; **P-value < 0.001 HS

Table 3 Cutoff levels of size and irregularity index

	Area under the curve	P-value	95% confidence interval		Cutoff	Sensitivity%	Specificity%
			Lower bound	Upper bound			
Maximum diameter (mm)	0.729	0.001*	0.600	0.859	8.8	74.5	62.5
Irregularity index	0.698	0.003*	0.568	0.827	1.9032	78.7	54.2
Peak frequency%	0.666	0.020*	0.526	0.806	20.5	56.3	79.2

P-value > 0.05 NS; *P-value < 0.05 S; **P-value < 0.001 HS



correlation between neoplastic and non-neoplastic nodules (Table 4). The cutoff level for peak frequency percentages was 20.5% with sensitivity and specificity of 56.3% and 79.2%, respectively (Table 3) (Fig. 1).

After nodule segmentation, the data analysis of histogram showed that there was no significant correlation between neoplastic and non-neoplastic nodules (Table 4).

The behavior after follow-up of the nodules

The behavior of the nodules was traced for 2 years. The progressive behavior was significantly associated with malignant nodules (Fig. 3) and regression with non-neoplastic nodules (P -value < 0.001) (Figs. 4 and 5) (Table 4). There were high sensitivity, specificity, and accuracy of the behavior of the nodule (66.7%, 100%, and 83.2%, respectively).

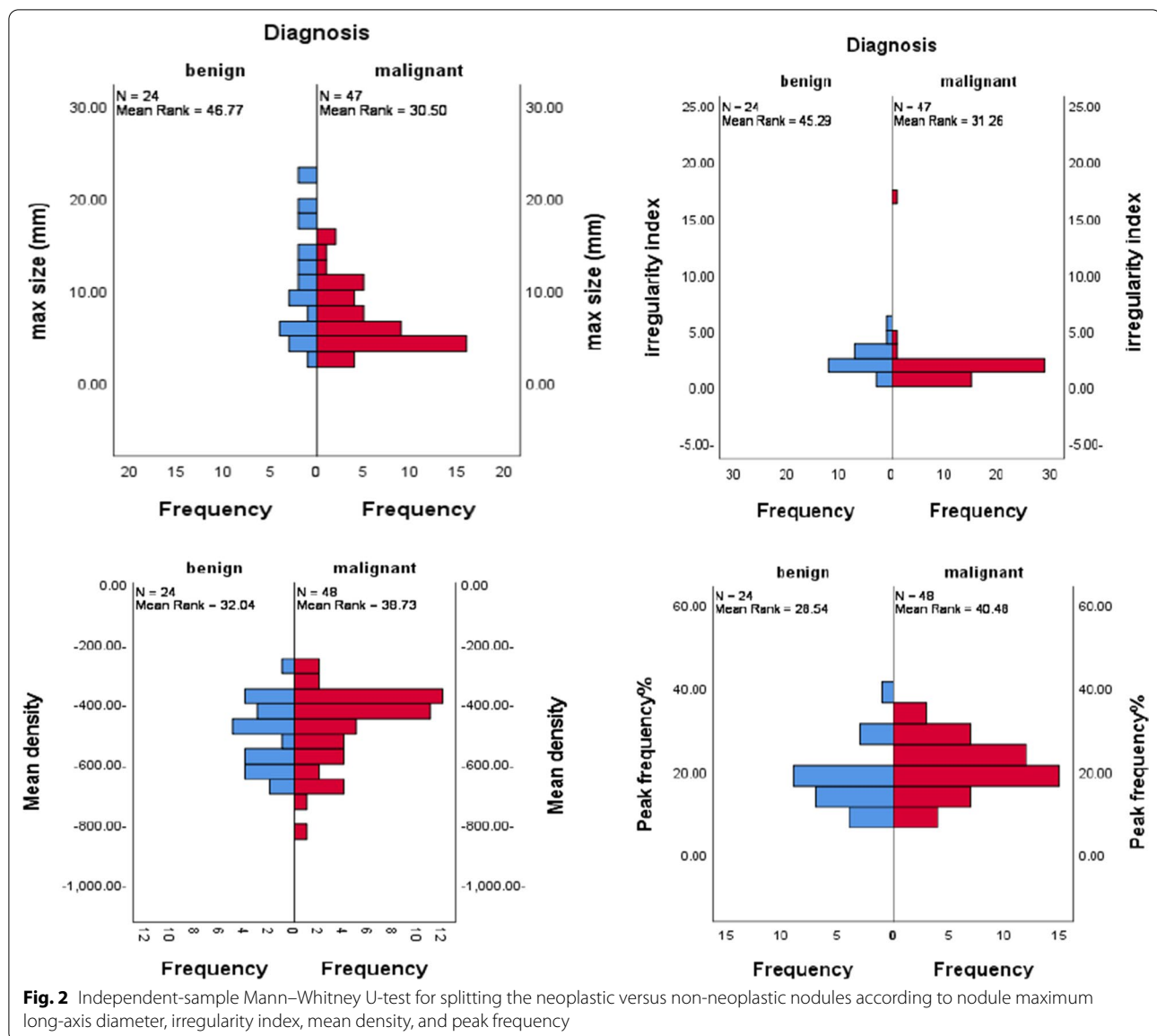
Discussion

Much progress had been made in cancer prevention and early detection, resulting in the reduction in mortality rates and improved survival rates [6]. Evangelista et al.'s study [8] showed a follow-up scheme guideline for pure GGNs detected cancer incidentally or at lung cancer screening. To be biennial, CT follow-up for GGN

must be less than 5 mm, annual for GGN 5–10 mm, and 3–6 months for GGN more than 10 mm. There must also be a downgrading of CT follow-up for stable nodules and upgrading of CT follow-up duration for nodules that increase in size and/or density. Nodules after 3–6 months follow-up that increased in size necessitate surgical resection. There must be continuous CT surveillance using unenhanced, low-dose techniques until life expectancy.

In this study, we evaluated CT chest scans of 72 patients, and 33.3% were non-neoplastic nodules. All of them were inflammatory, yet 66.7% were neoplastic nodules. Correlation of lesion size, behavior, density, shape, and histogram analysis with the final diagnosis provides basic features for pulmonary nodules, which help in determining the likelihood of these nodules representing neoplastic disease.

According to the current international guidelines, size and growth rate represented the main indicators to determine the nature of a pulmonary nodule, but the first radiological predictor of malignancy is the size [9, 10]. In this study, there was statistically significant relation between mean size of the nodule and final diagnosis. The mean long-axis diameter in cases of malignant nodules was



6.66 mm, yet the mean long-axis diameter of benign nodules was 11.25 mm (P -value < 0.002). This was explained that the nodules were pGGNs, and the neoplastic pGNN is detected more in preinvasive lesions, which is the early stage and small in size, which when it increases in size, solid component increased and will be excluded from this study. Truong et al. [11] reported that in terms of size, the likelihood of malignancy positively correlates with nodule diameter. As the diameter of a nodule increases, so does the likelihood of malignancy; however, a small nodule diameter does not exclude malignancy. Small nodules (<4 mm) have less than 1% chance of being malignant. Furthermore, the risk for malignancy increases to 10–20% for nodules with the size of 8 mm.

Nodule growth, determined by imaging surveillance, could be used as a diagnostic tool for assessing malignancy [12–14]. Truong et al.'s study showed that after reassessing the nodule with CT, lesions that resulted from infectious or noninfectious inflammatory causes mostly regressed or resolved in the interval; however, nodule increased in diameter in follow-up and the risk of malignancy increased. Therefore, follow-up was the only strong predictor for malignancy with sensitivity and specificity of 71% and 95%, respectively [15]. Moreover, persistent partial nodules are more likely to be malignant, but they may also be benign like in cases of focal interstitial fibrosis and organizing pneumonia. Kim et al.'s study [16] also showed that 75% of persistent

Table 4 Relation between data analysis of the histogram and follow-up behavior of the segmented neoplastic and non-neoplastic pulmonary nodules

	Diagnosis				P-value
	Benign		Malignant		
	Count	%	Count	%	
Visual assessment of the CT histogram					
α type	14	58.3%	20	41.7%	0.182
β type	10	41.7%	28	58.3%	0.182
Skewness					
Negative to the left	12	50.0%	29	60.4%	0.400
Symmetrical (0)	6	25.0%	15	31.3%	0.582
Positive to the right	6	25.0%	4	8.3%	0.074
Kurtosis					
Negative	5	20.8%	9	18.8%	1
0	6	25.0%	18	37.5%	0.289
Positive	13	54.2%	21	43.8%	0.404
Number of peaks					
0	4	16.7%	2	4.2%	0.146
1	5	20.8%	5	10.4%	
2	10	41.7%	27	56.3%	
3	5	20.8%	14	29.2%	
Behavior after follow-up					
Stationary	1	4.2%	3	6.3%	<0.001**
Progressive	0	0.0%	42	87.5%	
Regressive	23	95.8%	3	6.3%	

P-value > 0.05 NS; *P-value < 0.05 S; **P-value < 0.001 HS

ground-glass appearance was malignant in origin. They explained this great variation by the different types of the original malignancy. In a small study, Lindell et al. reported that 11 out of 18 malignant nodules showed a primary decrease in size at some point on their growth curves.

The nodule appearance in terms of density affects the probability of malignancy, reflecting histological differences between lesions [11, 15]. In this study, regarding pGGNs, there was no statistically significant relation between mean density with the final diagnosis. The prevalence of malignancy was higher among solid lung nodules, particularly when considering semisolid than solid ones [17]. Yet, malignant nodules mostly have a lepidic growth pattern (which arises from and spread along alveolar walls without invasion), which there is an inclusion of air or an air bronchogram or degenerative changes such as necrosis or hemorrhage within the tumor. Fat attenuation (− 40 to − 120 HU) is frequently seen in as many as 50% of neoplasms at CT. Other causes of fat attenuation in pulmonary nodules included pulmonary metastases [11].

Zhang et al. [18] found statistically significant density deviation in the nonsolid component that may help to identify invasive GGNs. The MIA and IA and the mean, maximum, and minimum density and density deviation had a positive correlation over time, while benign and preinvasive GGNs showed a negative correlation for these features. A diagnostic model based on three GGN features (increasing in diameter, mean density, and density deviation) identified invasive GGNs with a sensitivity, specificity, and area under the ROC curve (AUC) of 83.7%, 61.9%, and 0.786, respectively ($P < 0.001$). This was consistent with this study that showed the change in density over time was significantly affecting the diagnosis as the mean density of persistent neoplastic lung nodules was − 91.52 HU with cutoff level − 99.5 HU. However, in cases of benign nodule, it was − 247.13 HU after nodule follow-up ($P < 0.001$).

Regarding nodule multiplicity, in a study in the University of Chicago Medical Center, they postulated high statistically significant correlation between multiplicities of nodules and increased likelihood of malignancy [10]; however, in this study, there was no significant relation to nodule multiplicity.

The morphological features of lung nodules had a great role in defining whether it is malignant or benign [15]. According to this study, there was a significant positive relationship between the shape and margin of nodules in the CT chest and increases their susceptibility to be malignant. The regular and well-defined lung nodules are highly significantly related to malignant ($P < 0.001$ and 0.019, respectively). Metastatic nodules often exhibit a largely uniform growth rate and homogenous invasion in all directions. These features contribute to a round or quasi-circular contour, whereas nonmetastatic lesions, including benign lesions and primary lung cancer, have irregular shapes due to uneven growth rates at various sites [19]. Metastatic etiology exceeded primary adenocarcinoma in this study. Truong et al. stated that benign conditions that resulted from infection or inflammation, focal atelectasis, tuberculoma, and progressive massive fibrosis may also have a speculated margin. In addition, smooth margins do not exclude malignancy; as many pulmonary metastasis as 20% of primary lung malignancies have smooth margins [11]. Chun et al. reported that both benign and malignant nodules could exhibit smooth edges [13]. Moreover, this was in agreement with Tsutsui who found that 87% of focal pure ground-glass opacities (GGOs) had a well-defined border or round shape. Nambu et al.'s study showed that a well-defined border and rounded shape of focal GGO is more frequently seen in neoplastic lesions (well-differentiated adenocarcinoma) than in non-neoplastic inflammatory lesions [6, 20].

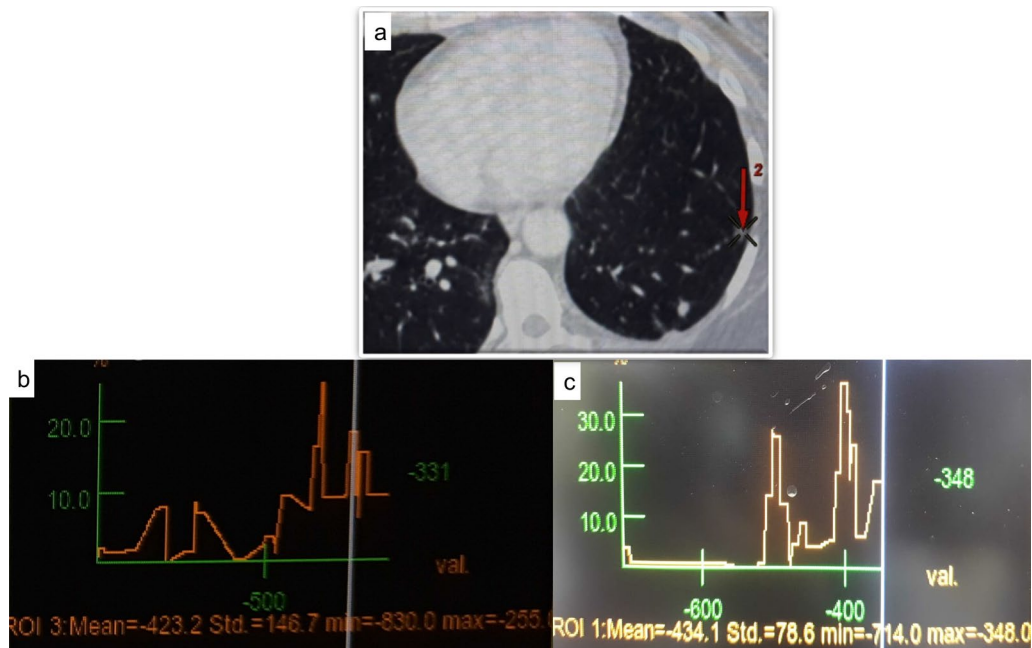


Fig. 3 **a** Axial CT scan (lung window) was done for metastatic workup of the patient, showed a peripheral left upper lobe ground-glass pulmonary nodule, **b** CT histogram for the segmented nodule. GGN showed type α (sharp peak at low CT value), mean density: -423.2 HU, maximum density: -255 HU, minimum density: -830 HU, STD: 146.7 , and skewness was negative. Kurtosis was positive with peak frequency 24% . **c** Note the changes on follow-up after 2 years as follows: histogram of the segmented GGN showed type β , mean density: -434.1 HU, maximum density: -348 HU, minimum density: -714 HU, STD: 78.6 , skewness is negative, and kurtosis is positive with peak frequency 36%

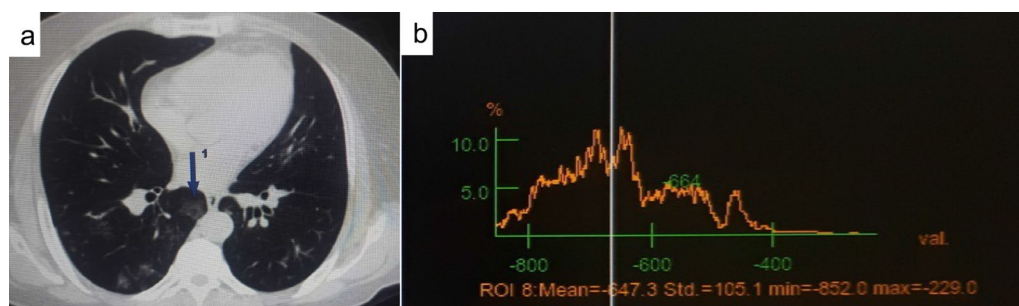


Fig. 4 A 62-year-old male. **a** CT scan (lung window) showed few GGNs, the illustrated one was seen at the right lower lobe, clinical and laboratory diagnosis of chest infection, with disappearance of nodule after 2 weeks. **b** CT histogram for the segmented GGN, CT exam showed mean density: -647.3 HU, maximum density: -229 HU, minimum density: -852 HU, STD: 105.1 , skewness was negative, kurtosis was zero, two peaks with peak frequency 11% , and visual assessment of CT histogram of ROI is type β

In recent years, several studies had applied texture analysis of GGNs. In this study, there was statistically significant correlation between peak frequency percentage of the histogram and the final diagnosis with no significant result regarding other performed visual assessment of histogram features. To the best of our knowledge, this study is the first to study the relationship between histogram features as qualitative assessment of kurtosis, skewness, and peak frequency percentage measures for evaluating pGGNs. We expected that skewness or

kurtosis would help distinguish the neoplastic pGGNs from benign pGGNs. However, the distinction was not accomplished with skewness and kurtosis. Chae et al. [21] found that higher kurtosis and smaller mass are significant differentiators of preinvasive lesions from invasive pulmonary aspergillosis; however, they only focused on partly solid GGOs and few texture features, as histogram, volumetric, and morphological features. According to Mao et al., regarding the histogram analysis between benign and malignant in all types of pulmonary

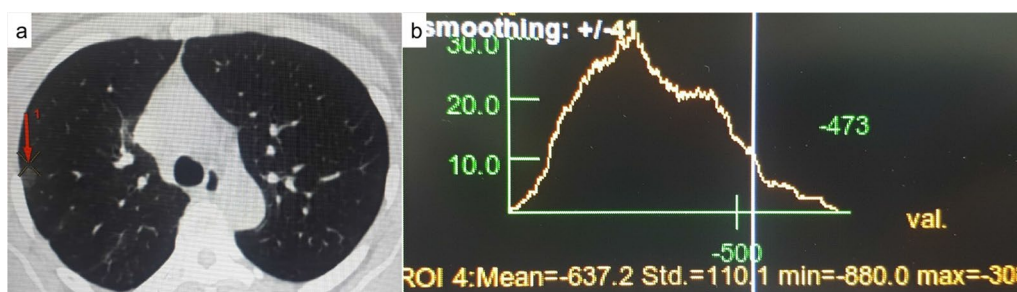


Fig. 5 A 49-year-old. **a** NECT scan showing few GGO, the illustrated one was seen at the right upper lobe, clinical and laboratory diagnosis of chest infection, with disappearance of nodule after 2 weeks. **b** CT histogram for the segmented GGO showed mean density: -637.2 HU, maximum density: -308 HU, minimum density: -880 HU, STD: 110.1 , skewness was zero, kurtosis was zero, one peak with peak frequency 30% , and visual assessment of CT histogram of ROI was type

nodules, there was a significant difference found in the kurtosis values. The greater kurtosis and reduced skewness in malignant nodules may be related to the greater heterogeneity than benign nodules, although they appear to be uniformly solid nodules on CT images. These differences in internal density homogeneity are reflected by the differences in the kurtosis measurements but are not detected by conventional visual assessments [22].

Further studies are recommended for pGGNs on large-scale cases with more quantitative measures of histogram to be measured, comprehensive and robust radiomics evaluation which is a limitation in this study as it was not applicable in our workstation.

Conclusions

The pGGNs had special characteristics. Morphological and histogram-related CT chest features played an important role in discriminating neoplastic pGGNs from non-neoplastic pGGNs. All the parameters of mean nodule size, growth pattern, mean density, morphological features, nature, and peak percentage of the histogram analysis in pGGNs should be used in combination for nodule characterization.

Other helpful features like kurtosis and skewness need multicenter studies to get full benefit and develop the final guidelines to follow.

Abbreviations

GGO: Ground-glass opacity; CT: Computed tomography; HU: Hounsfield unit; kV: Kilovoltage; mA: Milliampere; SD: Standard deviation.

Acknowledgements

Not applicable.

Author contributions

AME, MAK, MRA and MAH reviewed the CT images. AME, MRA and MAH wrote the manuscript. AME, MAK, MRA, YHE analyzed and interpreted the patient data. MAH reviewed and submitted the manuscript. All authors have read and approved the manuscript.

Funding

No funding was obtained for this study.

Availability of data and materials

The datasets used and/or analyzed during the current study are available from the corresponding author on reasonable request.

Declarations

Ethics approval and consent to participate

Approval of the ethical committee of the 'Radiology department, Faculty of Medicine, Cairo University' was granted before conducting this prospective study; Reference number: not applicable. Local institutional review board approval was granted before conducting this cross-sectional study, and written informed consent was obtained from all patients.

Consent for publication

All patients included in this research gave written informed consent to publish the data contained within this study. If the patients were less than 16-year-old, deceased, or unconscious when consent for publication was requested, written informed consent for the publication of this data was given by their parents or legal guardians.

Competing interests

The authors declare that they have no competing interests.

Author details

¹Diagnostic Radiology and Intervention Department, Kasr Al-Ainy Faculty of Medicine - Cairo University, Al-Manial, Cairo 11559, Egypt. ²Pulmonary Medicine Department, Faculty of Medicine - Cairo University, Cairo, Egypt.

Received: 1 September 2022 Accepted: 23 November 2022

Published online: 30 November 2022

References

1. Lam S, Bryant H, Donahoe L, Domingo A, Earle C, Finley C et al (2020) Management of screen-detected lung nodules: a Canadian partnership against cancer guidance document. *Can J Respir Crit Care Sleep Med* 4:236–265. <https://doi.org/10.1080/24745332.2020.1819175>
2. Sun Y, Li C, Jin L, Gao P, Zhao W, Ma W et al (2020) Radiomics for lung adenocarcinoma manifesting as pure ground-glass nodules: invasive prediction. *Eur Radiol* 30:3650–3659. <https://doi.org/10.1007/s00330-020-06776-y>
3. Hong D, Xu K, Zhang L, Wan X, Guo Y (2020) Radiomics signature as a predictive factor for EGFR mutations in advanced lung adenocarcinoma. *Front Oncol* 10:28. <https://doi.org/10.3389/fonc.2020.00028>

4. Peng M, Li Z, Hu H, Liu S, Xu B, Zhu W et al (2016) Pulmonary ground-glass nodules diagnosis: mean change rate of peak CT number as a discriminative factor of pathology during a follow-up. *Br J Radiol* 89:20150556. <https://doi.org/10.1259/bjr.20150556>
5. Park CM, Goo JM, Lee HJ, Lee CH, Chun EJ, Im JG (2007) Nodular ground-glass opacity at thin-section CT: histologic correlation and evaluation of change at follow-up. *Radiographics* 27:391–408. <https://doi.org/10.1148/rgr.272065061>
6. Li WJ, Lv FJ, Tan YW, Fu BJ, Chu ZG (2021) Pulmonary benign ground-glass nodules: CT features and pathological findings. *Int J Gen Med* 14:581–590. <https://doi.org/10.2147/IJGM.S298517>
7. Lubner MG, Smith AD, Sandrasegaran K, Sahani DV, Pickhardt PJ (2017) CT texture analysis definitions, applications, biologic correlates, and challenges. *Radiographics* 37:1483–1503. <https://doi.org/10.1148/rgr.2017170056>
8. Evangelista L, Panunzio A, Scagliori E, Sartori P (2018) Ground glass pulmonary nodules: their significance in oncology patients and the role of computer tomography and 18F-fluorodeoxyglucose positron emission tomography. *Eur J Hybrid Imaging* 2:2. <https://doi.org/10.1186/s41824-017-0021-z>
9. Larici AR, Farchione A, Franchi P, Ciliberto M, Cicchetti G, Calandriello L, Del Ciello A, Bonomo L (2017) Lung nodules: size still matters. *European Respir Rev Off J European Respir Soc* 26(146):170025. <https://doi.org/10.1183/16000617.0025-2017>
10. Li F, Armato SG, Giger ML, MacMahon H (2016) Clinical significance of noncalcified lung nodules in patients with breast cancer. *Breast Cancer Res Treat* 159:265–271. <https://doi.org/10.1007/s10549-016-3937-2>
11. Truong MT, Ko JP, Rossi SE, Rossi I, Viswanathan C, Bruzzi JF et al (2014) Update in the evaluation of the solitary pulmonary nodule. *Radiographics* 34:1658–1679. <https://doi.org/10.1148/rgr.346130092>
12. Zhao YR, Heuvelmans MA, Dorrius MD, van Ooijen PM, Wang Y, de Bock GH et al (2014) Features of resolving and nonresolving indeterminate pulmonary nodules at follow-up CT: the Nelson study. *Radiology* 270:872–879. <https://doi.org/10.1148/radiol.13130332>
13. Chun EJ, Lee HJ, Kang WJ, Kim KG, Goo JM, Park CM et al (2009) Differentiation between malignancy and inflammation in pulmonary ground-glass nodules: the feasibility of integrated 18F-FDG PET/CT. *Lung Cancer* 65:180–186. <https://doi.org/10.1016/j.lungcan.2008.11.015>
14. Gould MK, Fletcher J, Lannetoni MD, Lynch WR, Midhun DE, Naidich DP et al (2017). Evaluation of patients with pulmonary nodules: when is it lung cancer?: ACCP evidence-based clinical practice guidelines (2nd edition). *Chest*, 132:1085–1305. <https://doi.org/10.1378/chest.07-1353>
15. Xu DM, van der Zaag-Loonen HJ, Oudkerk M, Wang Y, Vliegenthart R, Scholten ET et al (2009) Smooth or attached solid indeterminate nodules detected at baseline CT screening in the Nelson study: cancer risk during 1 year of follow-up. *Radiology* 250:264–272. <https://doi.org/10.1148/radiol.2493070847>
16. Kim HY, Shim YM, Lee KS, Han J, Yi CA, Kim YK (2007) Persistent pulmonary nodular ground-glass opacity at thin-section CT: histopathologic comparisons. *Radiology* 245:267–275. <https://doi.org/10.1148/radiol.2451061682>
17. Yankelevitz DF, Yip R, Smith JP, Liang M, Liu Y, Xu DM, Writing Committee for The International Early Lung Cancer Action Program Investigators Group et al (2015) CT screening for lung cancer: nonsolid nodules in baseline and annual repeat rounds. *Radiology* 277:555–564
18. Zhang YP, Heuvelmans MA, Zhang H, Oudkerk M, Zhang GX, Xie XQ (2018) Changes in quantitative CT image features of ground-glass nodules in differentiating invasive pulmonary adenocarcinoma from benign and in situ lesions: histopathological comparisons. *Clin Radiol* 73:504.e9–504.e16. <https://doi.org/10.1016/j.crad.2017.12.011>
19. Hu T, Wang S, Xiangyu E, Yuan Y, Huang L, Wang J et al (2019) CT morphological features integrated with whole-lesion histogram parameters to predict lung metastasis for colorectal cancer patients with pulmonary nodules. *Front Oncol* 9:1241. <https://doi.org/10.3389/fonc.2019.01241>
20. Tsutsui S, Ashizawa K, Minami K, Tagawa T, Nagayasu T, Hayashi T et al (2010) Multiple focal pure ground-glass opacities on high-resolution CT images: clinical significance in patients with lung cancer. *Am J Roentgenol* 195:W131–W138. <https://doi.org/10.2214/AJR.09.3828>
21. Chae HD, Park CM, Park SJ, Lee SM, Kim KG, Goo JM (2014) Computerized texture analysis of persistent part-solid ground-glass nodules: differentiation of preinvasive lesions from invasive pulmonary adenocarcinomas. *Radiology* 273:285–293. <https://doi.org/10.1148/radiol.14132187>
22. Mao L, Chen H, Liang M, Li K, Gao J, Qin P et al (2019) Quantitative radiomic model for predicting malignancy of small solid pulmonary nodules detected by low-dose CT screening. *Quant Imaging Med Surg* 9:263–272. <https://doi.org/10.21037/qims.2019.02.02>

Publisher's Note

Springer Nature remains neutral with regard to jurisdictional claims in published maps and institutional affiliations.

Submit your manuscript to a SpringerOpen[®] journal and benefit from:

- Convenient online submission
- Rigorous peer review
- Open access: articles freely available online
- High visibility within the field
- Retaining the copyright to your article

Submit your next manuscript at ► [springeropen.com](https://www.springeropen.com)